Light-Induced Forward and Reverse Intersystem Crossing in Green Fluorescent Proteins at Cryogenic Temperatures

Lukas Rane, Jip Wulffele, Dominique Bourgeois, Oleksandr Glushonkov, Angela Mantovanelli, Ninon Zala, Martin Byrdin

THE JOURNAL OF PHYSICAL CHEMISTRY B
A JOURNAL OF THE AMERICAN CHEMICAL SOCIETY

pubs.acs.org/JPCB

Article

Light-Induced Forward and Reverse Intersystem Crossing in Green Fluorescent Proteins at Cryogenic Temperatures

Lukas Rane, Jip Wulffele, Dominique Bourgeois, Oleksandr Glushonkov, Angela M. R. Mantovanelli, Ninon Zala, and Martin Byrdin*

Cite This: https://doi.org/10.1021/acs.jpcb.3c02971

Read Online

ACCESS | Metrics & More | Article Recommendations

ABSTRACT: Combining fluorescence and phosphorescence kinetics, we characterize forward and reverse intersystem crossing (FISC and RISC, respectively) between the singlet and triplet manifolds S ↔ T in photoswitchable (rsEGFP2) and non-photoswitchable (EGFP) green fluorescent proteins upon continuous 488 nm laser excitation at cryogenic temperatures (CTs). Both proteins behave very similarly, with T_1 absorption spectra showing a visible peak at 490 nm (10 mM^{-1} cm^{-1}) and a vibrational progression in the near-infrared (720 to 905 nm). The dark lifetime of T_1 is 21−24 ms at 100 K and very weakly temperature-dependent up to 180 K. Above 180 K, T_1 lifetimes reduce rapidly to few milliseconds as found at room temperature (RT). FISC and RISC quantum yields are 0.3 and 0.1%, respectively, for both proteins. The light-induced RISC channel becomes faster than the dark reversal at power densities as low as 20 W cm^{-2}. We discuss implications for fluorescence (super resolution-) microscopy at CT and RT.

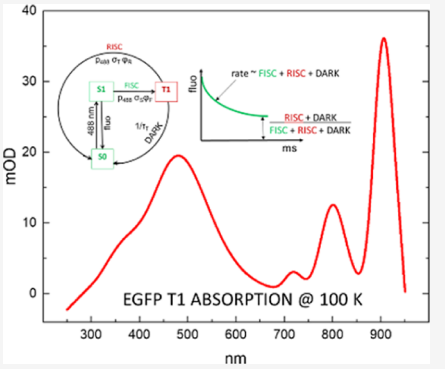

INTRODUCTION

Cryogenic light microscopy has become increasingly popular in biology mainly for two reasons: less harsh sample preservation conditions than those resulting from chemical fixation and increased resistance of the employed fluorescent markers to photobleaching.[1,2] Especially in the context of rapidly developing CLEM (correlated light and electron microscopy), where the light microscope serves to identify those sample portions that deserve to be further investigated by electron microscopy (EM), a sufficiently resolved fluorescence image under cryo-EM conditions is desirable.[3,4] The resulting efforts to develop cryo-super-resolution microscopy are accompanied by the search for suitable fluorescent markers that can be photoswitched at cryogenic temperatures (CTs).[5−9]

The uncontestable observation of longer resistance to photobleaching both for fluorescent proteins (FPs) in whole cells[1] and for organic dyes in buffer solution[2] could be explained either by the lack of some ingredients necessary for photobleaching processes due to diffusion slowed by CT or by the temperature-induced slowing of some intramolecular processes involved in photobleaching.[10] As to the latter, we recently proposed for some green fluorescent protein (GFP)-type proteins an entrance gateway to photochemical bleaching via the triplet state.[11] Intriguingly, we also observed that the decay of that triplet state accelerates about twice upon heating from 10 to 40 °C. From this effect, we concluded that the decay pathway proceeds via an uphill step with an apparent activation barrier of 0.26 ± 0.02 eV. Based on this finding, at CTs, a substantially longer triplet lifetime and, as a consequence of high reactivity of the triplet state, also an increased propensity for some bleaching pathways could be expected. In order to illuminate this discrepancy, we seek to experimentally establish values for triplet state lifetime and formation quantum yield of some popular GFPs at CTs.

Historically, the FP triplet state was believed to be microsecond-lived at ambient conditions. This assumption was based on the analogy to the typical behavior of organic dyes and on the observation of microsecond-lived reversible dark states in fluorescence correlation spectroscopy measurements.[12] The true nature of these microsecond-lived reversible dark states remains to be finally clarified; most probably, they are linked to changes in the isomerization and/or protonation state of the GFP chromophore.[13] Regardless of their chemical identity, the D-Rex concept (dark state relaxation), using microsecond-interleaved illumination schemes that allow relaxation of these dark states to the ground state, afforded a more than tenfold signal increase in stimulated emission depletion (STED)-type measurements with MHz excitation.[14]

Received: May 5, 2023
Revised: May 12, 2023

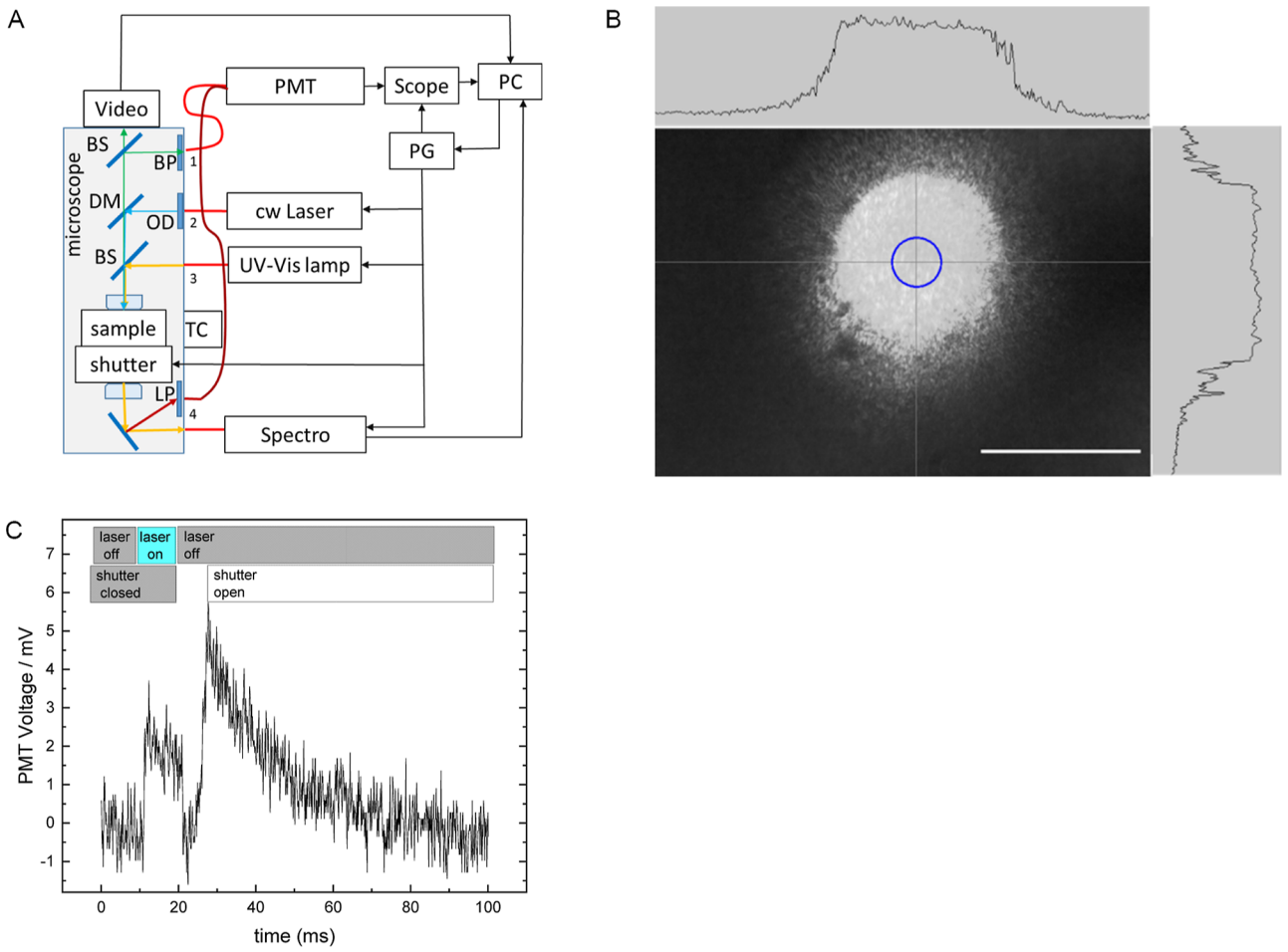

Figure 1. Opto-mechanico-electrical setup for submillisecond-resolved detection of absorption/emission of microscopic samples at CTs (CAL(AI)^{2}DOSCOPE). (A) Scheme of the setup. Black lines represent electrical connections; red lines, optical fibers; and all other colors, open air light path. BS: beam splitter, BP: bandpass filter, DM: dichroic mirror, LP: longpass filter >650 nm, OD: neutral density filter, PC: personal computer, PG: pulse generator, PMT: photomultiplier tube, and TC: temperature control. The dark red fiber is used for phosphorescence detection via channel 4 instead of fluorescence detection via channel 1. (B) Excitation beam profile. The diameter at half height is 120 μm. The blue circle in the center (30 μm diameter) is the spot illuminated for the absorption measurement (200 μm fiber diameter); the fluorescence detection spot is half that size (100 μm fiber, 15 μm spot). Scale bar: 100 μm. (C) Pulsing scheme and time trace for phosphorescence detection. The 2 mV signal from 11 to 21 ms is diffused laser light reaching the detector regardless of closed shutter and notch filter. The period from 21 to 28 ms is the time it takes the shutter to open completely. Therefore, the initial part of the phosphorescence decay is not detected.

Unequivocal identification of the enhanced GFP (EGFP) triplet state by observation of millisecond-lived phosphorescence revealed that its actual lifetime is three orders longer than previously anticipated, in hindsight not completely unexpected due to the shielded position of the GFP chromophore inside the tight protein barrel.[11] Such long-lived dark states were bound to escape confocal detection, whose accessible time window is limited by diffusion to microseconds. Wide-field detection can overcome this limitation but the observed kinetics will still result from a superposition of intrinsic chromophore photophysics and diffusional exchange at the borders of the illuminated area. This exchange could be prevented by immobilization via embedding in gels, e.g., polyvinyl alcohol or polyacrylamide, but these procedures may still perturb observations of the desired states. Luckily, at cryo-temperatures, this exchange is slowed or completely stalled, so that millisecond photophysics should become directly observable in a wide-field setting. This perspective motivated us to improve the time resolution of our cryo-microspectrophotometer (CAL(AI)^{2}DOSCOPE[15]) by introducing modalities for both faster excitation-laser switching and fluorescence detection. As a consequence, we can now reliably resolve kinetics in the low millisecond time range, also relevant for an electron multiplying charge-coupled device or a scientific complementary metal-oxide semiconductor (sCMOS) camera acquisition exposure times. In this contribution, we follow the kinetic evolution of the fluorescence intensity level of two specific GFP-type fluorescent marker proteins during the first few milliseconds: EGFP and its reversibly switchable analogue rsEGFP2. The former is the one that served to establish room-temperature triplet state characteristics;[11] the latter has recently been proposed as a suitable candidate for cryoactivation-based microscopy.[5] Both prototypical FPs serve as benchmarks for the performance characterization of a steady stream of newly developed FPs of various colors and enhanced properties.[16,17] Here, we provide insight into two processes that decisively determine the performances of EGFP and rsEGFP2: light-induced formation and decay of the first excited triplet state T_1 (forward and reverse intersystem crossing, denoted FISC and

https://doi.org/10.1021/acs.jpcb.3c02971
J. Phys. Chem. B XXXX, XXX, XXX−XXX

RISC, respectively).[18−21] Strategies to enhance photostability by RISC enhancement have been proposed.[20] In EGFP, T_1 has been shown to live few milliseconds at room temperature (RT), and a T_1 absorption spectrum at RT has been measured,[11] but the dominant contribution of ground-state bleaching prevented the determination of the T_1 absorption coefficient at the popular excitation wavelength 488 nm.[11] Here, we make use of the cooling-induced lifetime prolongation of T_1 to measure its complete NUV−vis−NIR absorption spectrum at CT, immediately after a saturating pulse of 488 nm laser excitation. Moreover, we report the decay kinetics of the accompanying phosphorescence.

MATERIALS AND METHODS

Sample Preparation. Proteins were overexpressed and purified as previously described.[22] A tiny fraction of a 2 μL drop of a 1:1 mixture of a 2 mg/mL (ca. 0.1 mM) protein solution (50 mM HEPES, pH 7.5) with glycerol (final glycerol concentration estimated to 50%) was placed in a crystallographic loop and mounted on the magnetic sample holder of our cryo-microspectrophotometer CAL(AI)^{2}DOSCOPE.[15]

Apparatuses. Our cryogenic micro-spectrophotometer CAL(AI)^{2}DOSCOPE allows for simultaneous sample illumination/observation via a video camera (ueye, IDS Obersulm, Germany) and four separate optical channels (see Figure 1A for a schematic presentation of the setup). Here, we make use of channels 2 and 1 for laser excitation and fluorescence observation, respectively. A dichroic mirror (Di02-R488, Semrock) serves to separate the two: light from a fiber coupled (Avantes 0.6 mm Ø) Oxxius 488 nm laser (LBX-488-200) and fluorescence emission from the sample. Kinetic traces of fluorescence intensity upon laser exposure were recorded via a 512/25 bandpass filter (Semrock) and an additional notch filter (NF03-488E-25, Semrock). For this, the microscope output was fiber-coupled (Avantes 0.1 mm diameter) to a photomultiplier tube (PMT, Hamamatsu H13543-20) which in turn was coupled via a 100 kΩ load resistance to a LeCroy Wavejet 334A oscilloscope (DC—100 MHz bandpass). Laser exposition was controlled by a digital delay-pulse generator (9518, Quantum Composer) and had a rise time of 100 μs. For each condition (temperature, power density), a total of 64 illumination sequences were averaged at a frequency of 1 Hz and with durations varying from 4 to 16 ms laser exposition, followed by dark time. The initial signal amplitude did not decrease between subsequent illumination pulses of the acquisition series, indicating that photobleaching during averaging was negligible and dark recovery was completed. Sample temperature was controlled by an Oxford Cryosystems 600 gaseous nitrogen cryostat to a precision of ±0.1 K.

The remaining channels 3 and 4 serve for simultaneous white light illumination (Avantes) and absorption detection, respectively. The absorption spectrometer (Avantes) is additionally protected from laser illumination and sample fluorescence by a mechanical shutter (Thorlabs SH05R with driver SC10) that was also synchronized by the pulse generator.

To compensate for temporal drift and optical aberration at wavelengths >500 nm, these spectra were measured interleaved: alternatively, with laser on and with laser off. Three spectra of 7 ms exposure time each with laser off were followed accordingly by three spectra with laser on at 10, 17, and 24 ms after laser off-switching. From these latter three spectra, exponential extrapolation to time zero (moment of off-switching) allowed to reconstruct the T_1-S_0 difference absorption spectrum. For these experiments, we used the maximal obtainable protein stock concentration of 30 mg/mL.

For phosphorescence detection, the setup was modified as follows (Figure 1C): Instead of to channel 1, the PMT input was coupled via a 650 nm longpass filter to the output of channel 4 (dark red in Figure 1A), and the PMT output was coupled to the oscilloscope entrance set to 1 MΩ. With this setup, opening the shutter immediately after a saturating 10 ms laser pulse, allowed for the direct registration of the time course of phosphorescence decay. 256 single traces were averaged. The signal vanished when the longpass filter was replaced by the 512/25 nm bandpass filter thus excluding the possibility of delayed fluorescence.

Data Treatment. For the determination of excitation rates, excitation power for an illuminated sample spot of 120 μm diameter (Figure 1B) was measured at the sample position using a PM100D power meter with an S120C measuring head (Thorlabs). The excitation rate kX is the product of excitation photon flux density p_{488} and chromophore absorption cross section σ_S. For the proteins used here, the extinction coefficient at 488 nm is temperature dependent because upon cooling both absorption and fluorescence spectra are narrowed and blue-shifted (see Figure 2). Consequently, we used for epsilon 80% of the peak value reported for RT, i.e., 41.9 and 48.8 mM^{-1} cm^{-1} for EGFP and rsEGFP2, respectively.

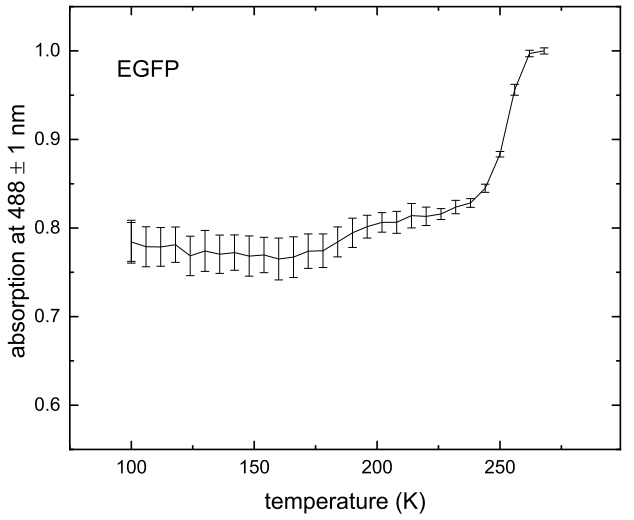

Figure 2. Absorption shift of EGFP upon cooling to 100 K. Error bars are s.d. from averaging over 487 to 489 nm. They are smaller above 240 K (peak) than below (flank).

For amplitude normalization, all experimental fluorescence decay curves at a given temperature were first fitted with an (exponential rise + exponential decay + offset)-model where all parameters are free except the time constant of the rise term that was shared among all curves. Subsequently, curves were normalized to the sum of decay phase amplitude and offset, thus assuring unity amplitude for full fluorescence onset and correcting for slight amplitude loss due to shutter opening kinetics (100 μs).

The thus-normalized curve families were fitted using a model consisting of a rise term with fixed amplitude (−1) and lifetime (100 μs) and a model of eq 4 in the Results section.

https://doi.org/10.1021/acs.jpcb.3c02971
J. Phys. Chem. B XXXX, XXX, XXX−XXX

RESULTS

We first determined the absorption spectrum of the reversibly populated triplet state. For this, we illuminated a protein sample at 100 K until saturation (20 ms), then stopped the laser and opened the shutter. At this moment, the sample contains a mixture of S_0 and T_1 state molecules.

Figure 3 shows the raw absorption spectra without any 488 nm laser illumination and immediately after its stopping, together with their difference (Figure 3B).

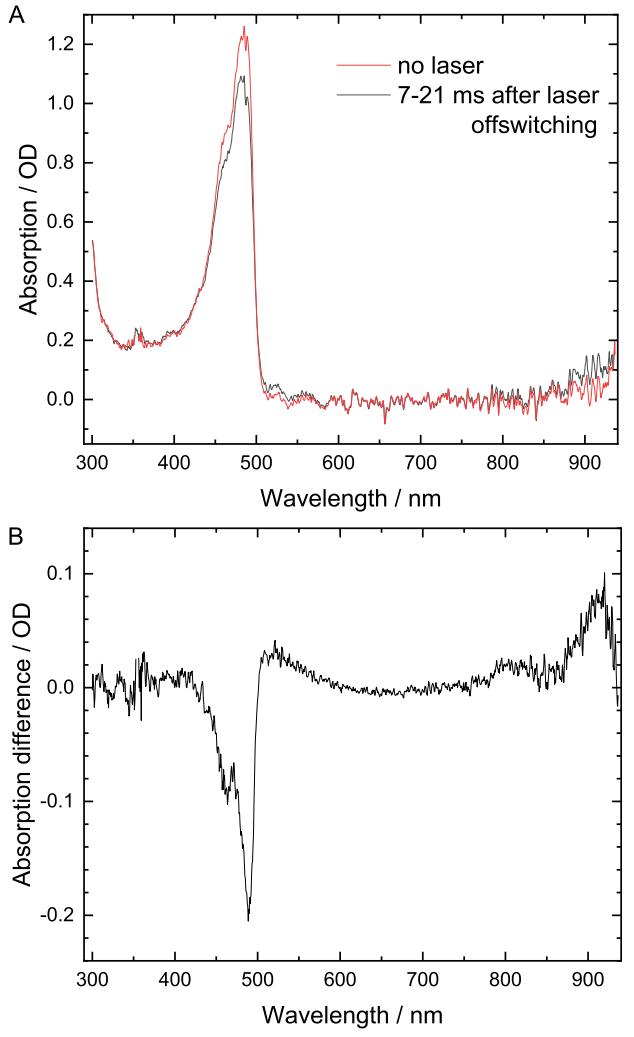

Figure 3. Absorption spectrum of EGFP at 100 K. Spectra were acquired alternatively with laser off (A, red) and laser on, rapidly after laser off-switching (A, black). The difference spectrum (B) is obtained by subtraction of the spectrum without illumination (A, red) from the first dark spectrum after laser off-switching (A, black). It contains ground-state bleaching (negative feature around 490 nm) and excited-state absorption (positive features to the left and right immediately around the ground-state bleach and in the near infrared above 700 nm).

Subtraction of an appropriate fraction (i.e., eliminating the 488 nm centered dip and reconstituting a positive Gaussian shape to the resulting band) of the ground-state absorption (Figure 3A, red) from the difference spectrum (Figure 3B) yielded the pure triplet state absorption spectrum (Figure 4A) that could be satisfactorily fitted by a sum of five Gaussians with peaks at 390, 490, 720, 800, and 905 nm. Fitting parameters are listed in Table 1.

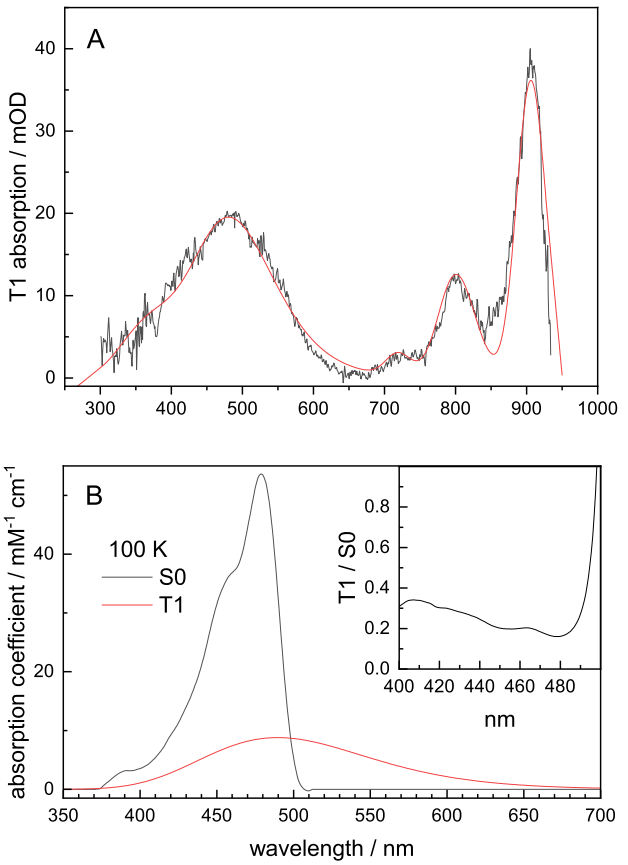

Figure 4. Absorption spectra of rsEGFP2 at 100 K. (A) Light minus dark difference spectrum at 20 ms after 488 nm illumination, corrected for the weighted contribution of ground-state (S_0) bleaching (black); fit with 5 Gaussians (red, see also Table 1); (B) S_0 spectrum and the 490 nm centered band of the T_1 spectrum scaled to an epsilon scale using normalization at 278 nm. (inset) Ratio of the values in the main panel.

Table 1. Parameters of Fitting Five Symmetric (on an Energy Scale) Gaussians to the T_1 Absorption Spectrum in Figure 4A

peak position in nm	peak position in cm^{-1}	peak fwhm in cm^{-1}
390	25,621.65238	9337.55145
490	20,423.13753	5270.20272
720	13,895.34884	824.18702
800	12,486.32011	941.92802
905	11,036.25171	588.70501

Figure 4A shows the T_1 absorption spectrum of rsEGFP2 at 100 K. The spectrum of EGFP is indistinguishable from that of rsEGFP2 within our signal-to-noise ratio.

The T_1 absorption spectrum shows a hitherto not resolved vibronic progression in the near infrared, with an inter-sideband spacing of 1440 cm^{-1}, in good agreement with the 1340 cm^{-1} previously reported for the singlet chromophore absorption at 77 K.[23] In the visible, the spectrum is dominated by a large band, peaking at 490 nm and stretching from 400 to 600 nm, thus covering the whole of the S_0 absorption band as well. This overlap previously prevented the unequivocal

https://doi.org/10.1021/acs.jpcb.3c02971
J. Phys. Chem. B XXXX, XXX, XXX−XXX

determination of the shape and amplitude of the T_1 visible absorption band but has also an important consequence: light of any wavelength that is used to excite green fluorescence does not only pump a fraction of the singlet population into T_1 (FISC) but, at the same time, also pumps backward from there into the singlet manifold (RISC). The backward/forward RISC/FISC efficiency ratio is given by the ratio of the absorption coefficients of T_1 and S_0 at the excitation wavelength (Figure 4B, with the ratio as shown in the inset) and the FISC and RISC quantum yields φ_F and φ_R. Moreover, under a continuous incident photon flux with density p_{488}, the amount of T_1 population that is formed depends on the intrinsic triplet state lifetime τ_T. In the following, we describe an approach to extract simultaneously φ_F, φ_R, and τ_T, based on the measurement of millisecond fluorescence kinetics. We make use of our microspectrophotometer CAL-(AI)^{2}DOSCOPE[15] together with protein immobilization by low-temperature vitrification and a continuous 488 nm laser that can be switched at kHz frequency with a rise time of 100 μs, i.e., sufficiently fast to be separated from the ISC processes we strive to observe (see Materials and Methods section for details).

Scheme 1 shows the relevant photophysical processes for a FP under monochromatic illumination. Under conditions of fast equilibrium between S_0 and S_1, we need to consider only their (normalized) sum S. Fluorescence is a measure of the temporal evolution of this singlet-state population and is given by eq 1 (scheme 1A).

$$S(t) = 1 - A(1 - \exp(-kt)) \quad (1)$$

Scheme 1. Photophysics of GFP-type Proteins. (A) Simplified Two State Model; (B) Photophysical Parameters Affecting the Rate Constants for the Three Processes Constituting $k1$ (FISC) and $k2$ (RISC and DARK). Under Continuous Illumination, at Steady State, the T_1 State has Population and Absorption Comparable to Those of S_0. However, in View of Its Much Longer Lifetime and Higher Reactivity, it is the Most Probable Gateway to All Kinds of Photochemistry Including Slow Blinking, Switching, Bleaching Phenomena. Therefore, in Addition to the Two Arrows Leading Back to S_0, an Additional (mostly) Irreversible Decay Pathway k_{PC} is Shown. The Arrow is Dotted Because the Total Photochemistry Yield is Small in Comparison with the Former Two Channels

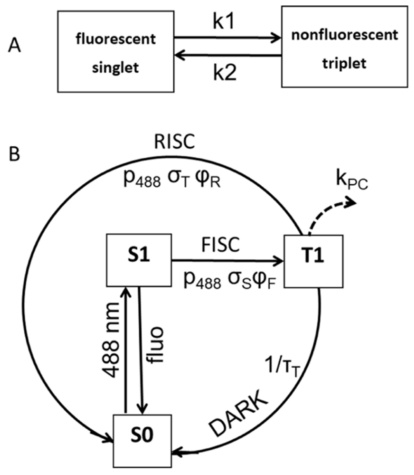

with (see scheme 1B)

$$[S](t = 0) = 1,\ k = (k1 + k2),\ A = k1/(k1 + k2) \quad (2)$$

At steady state (i.e., after having reached the kinetic plateau), we have $S = k2/(k1 + k2)$. Here, σ_S and σ_T are the absorption cross sections (in cm^2) of the singlet and triplet states, respectively, and relate to ε_S and ε_T (in M^{-1} cm^{-1}) by $\sigma_S = 1000 \ln 10\ \varepsilon_S/N_A$ and $\sigma_T = 1000 \ln 10\ \varepsilon_T/N_A$, where N_A is the Avogadro number.

Substituting

$$k1 = p_{488}\sigma_S\varphi_F,\ k2 = k_{RISC} + k_{DARK} = p_{488}\sigma_T\varphi_R + 1/\tau_T \quad (3)$$

into eq 2 and then eq 2 into eq 1, we obtain eq 4 that describes the fluorescence decay as a function of the rates of the FISC, RISC, and DARK processes (scheme 1B).

The resulting final fitting function has the form

$$S = 1 - \exp(-t/0.1) - 1/(1 + phiR \times \mathrm{eps} + 1/(kX \times tauT \times phiF/100))\, x(1 - \exp(-(kX \times phiF/100 \times (1 + phiR \times \mathrm{eps} + 1/(tauT \times phiF/100 \times kX)) \times t))) \quad (4)$$

where eps $= \sigma_S/\sigma_T$ is the ratio of the absorption cross sections of S_0 and T_1 at 488 nm, $kX = p_{488}$, σ_S is the excitation rate in kHz of the singlet ground state S_0, and the factor 100 converts the forward and reverse ISC quantum yields *phiF* and *phiR* to percent units.

Equation 4 thus provides an expression for fitting simultaneously φ_F, φ_R, and τ_T, knowing p_{488} from independent power measurements and both σ_S and σ_T values from Figure 4B. We then perform global fitting over data collected at various temperatures and excitation power densities. Preliminary "free" fits (no parameter sharing among datasets) indicated that upon temperature variation, *phiF* and *phiR* tended to be constant, whereas *tauT* varied systematically. Therefore, in the following, simultaneous fits at various temperatures were performed, where of the three free parameters *tauT*, *phiF*, and *phiR*, *phiF* and *phiR* were shared across temperatures and energies, whereas *tauT* was allowed to vary as a function of temperature (but not power density), yielding robust results.

Figures 5 and 6 show such fits for rsEGFP2 (Figure 5) and EGFP (Figure 6). The fitted parameters for both proteins are very similar and are given in Table 2, together with the EGFP literature values at RT for comparison.

Figure 7 shows the temperature dependence for τ_T for both proteins (solid symbols). The approach to assign the temperature dependence to the dark lifetime rather than to the forward and reverse quantum yield is justified, and the found values confirmed by comparison to the fitted lifetimes of phosphorescence decay kinetics for rsEGFP2 (open symbols in Figure 7) that do not depend on any assumptions.

DISCUSSION

We observed a rapidly reversible dark state and measured its lifetime and absorption spectrum. The identical decay times observed directly via phosphorescence and indirectly via fluorescence quenching kinetics indicate that in both cases the observed dark state is T_1 and that the spectra in Figure 4 and parameters in Tables 1 and 2 apply indeed to the first

https://doi.org/10.1021/acs.jpcb.3c02971
J. Phys. Chem. B XXXX, XXX, XXX−XXX

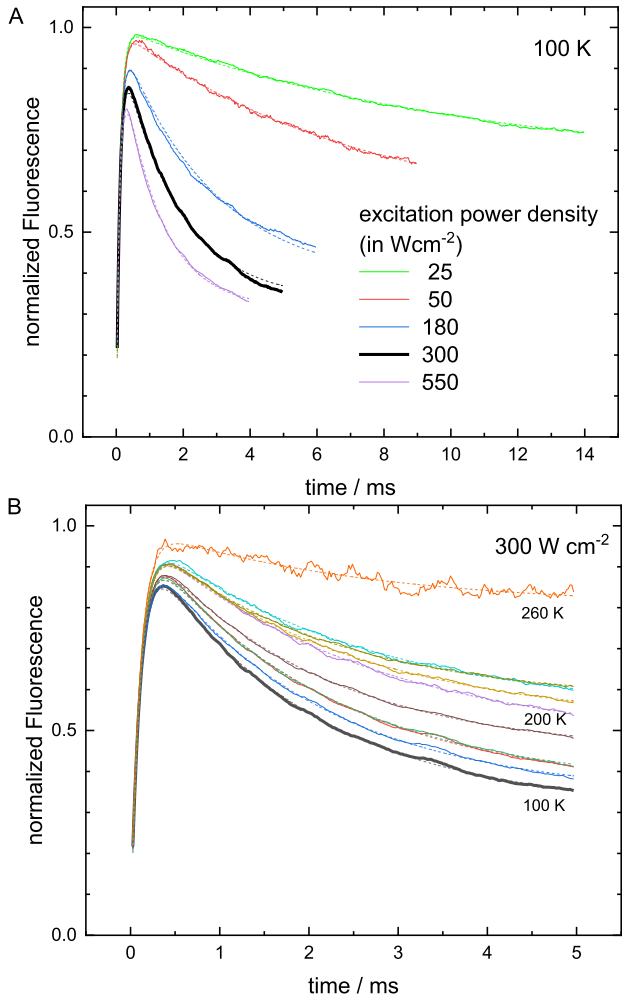

Figure 5. Time traces of the first milliseconds of fluorescence of dark-adapted rsEGFP2. (A) Various 488 nm excitation power densities at 100 K. (B) Various temperatures (increasing in 20 K steps) at 300 W cm^{-2} excitation power density. The thick black curves in panels A and B are the same. Dashed lines are fits using eq 4 and parameters as indicated in Table 1, last line.

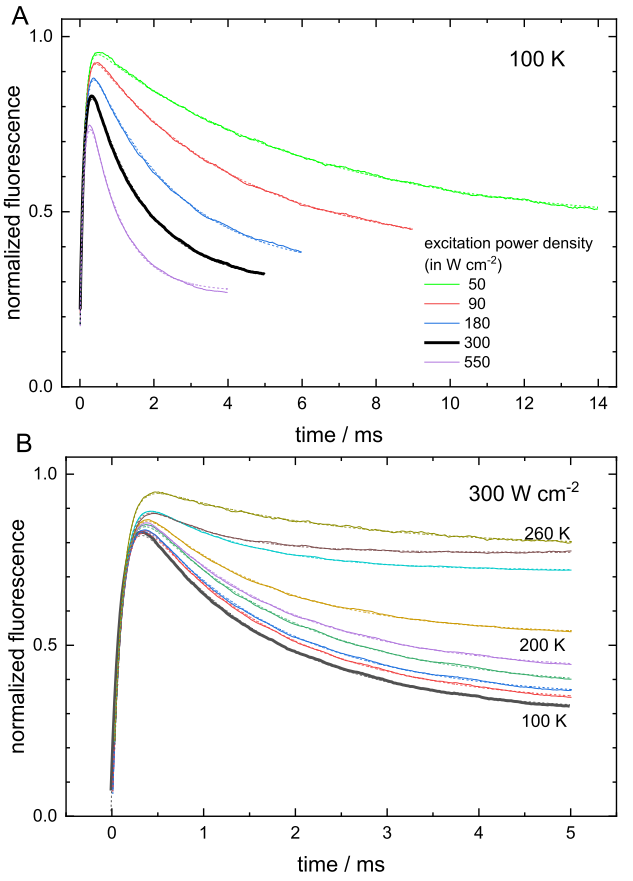

Figure 6. Time traces of the first milliseconds of EGFP fluorescence of a dark-adapted sample. (A) Various excitation power densities at 100 K. (B) Various temperatures (increasing in 20 K steps) at 300 W cm^{-2} excitation power density. The thick black curves in panels A and B are the same. Dashed lines are fits using eq 4 and parameters as indicated in Table 1, line 2.

excited triplet state. Although rsEGFP2 is known to cis/trans isomerize at RT, we argue that in the states we observe in this work the chromophore is always in its anionic cis conformation. T_1 is formed from its precursor S_1 that in turn is formed from S_0. The only form of the chromophore that contributes to fluorescence is the anionic cis conformation. Full recovery during the 1 s dark period testifies against accumulation of slowly switched species in appreciable amount. If any, these cannot correspond to isomerized or protonated states but would be radical states building up from intramolecular electron transfer as described in detail by Mantovanelli et al. (no diffusion, pH dependence, or structural changes observable at CT).[5]

It appears that the intrinsic triplet lifetimes of EGFP and rsEGFP2 are only slightly temperature-dependent between 100 and 180 K, i.e., up to the glass transition temperature (T_g) of our 50% glycerol/water mixture.[24] Above 180 K, the lifetimes decrease rapidly by a factor of about 3 down to the RT values (see Figure 7B for an Arrhenius presentation of the data in Figure 7A). The absence of a clear Arrhenius-type behavior over the whole temperature range suggests that below T_g, a deactivation channel present above T_g is shut off. The remaining channel is most likely intramolecular as it should not be diffusion dependent. This channel remains probably available above T_g, but its lifetime is too long to outcompete the diffusion-limited oxygen-related intermolecular pathway that likely dominates at high temperatures. Importantly, the 20 ms-pathway prevailing below T_g limits triplet-state saturation and the accumulation of long-lived dark states, which would otherwise offset the observed increased photostability at CTs.[1,2] This temperature- and power-dependent change in triplet quenching pathways is reminiscent of the earlier described power-dependent change between dominant bleaching mechanisms at RT in the EosFP-derivated marker IrisFP.[25] Interestingly, a comparable dark state with a formation yield of 0.3% and a lifetime of 25 ms has been recently reported by Peng et al. for a YFP mutant at RT.[26] They ascribed their observation to a further downstream, possibly radical, state but the similar parameters suggest that it might have T_1 character as well.

We have found that in both non-switchable and reversibly switchable GFPs at CTs upon continuous laser illumination, a significant fraction of the potentially fluorescing chromophores rapidly enters the dark T_1 state with a lifetime that is comparable to typical exposure times of CCD or sCMOS cameras used in fluorescence microscopy of biological samples. Both amount and formation rate of this fraction increase with excitation power density and, for 488 nm excitation, become

https://doi.org/10.1021/acs.jpcb.3c02971
J. Phys. Chem. B XXXX, XXX, XXX−XXX

Table 2. Photophysical Parameters for RT (Literature) and CT (Our Fits) of Forward and Reverse ISC

protein and condition	singlet ground state S_0		first excited triplet state T_1		
	absorption coefficient at 488 nm ε_S in mM^{-1} cm^{-1}	forward ISC quantum yield φ_F in %	absorption coefficient at 488 nm ε_T in $mM^{-1}cm^{-1}$	reverse ISC quantum yield φ_R in %	dark lifetime τ_T in ms
EGFP RT	53[b]	1.0 ± 0.5[c]	10 ± 5[c]	n.d.[a]	5.6[c,g]
EGFP 100 K	41.9[d]	0.32 ± 0.04[d,e]	10 ± 2[d,f]	0.12 ± 0.02[d,e]	21 ± 2[d]
rsEGFP2 100 K	48.8[d]	0.27 ± 0.04[d,e]	10 ± 2[d,f]	0.12 ± 0.02[d,e]	24 ± 6[d]

[a]n.d. Not determined. [b]From ref 16 [c]From ref 11 [d]This work. [e]Mean ± S.D. from $n \geq 6$ datasets. [f]Range estimated from uncertainty in ε_S contribution. [g]Value in the absence of oxygen.

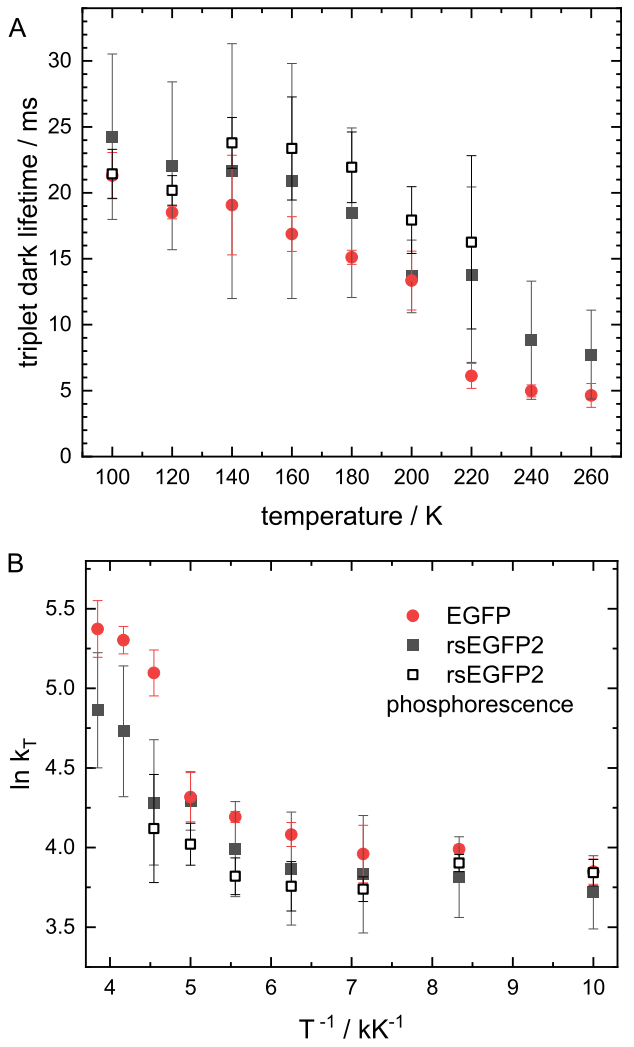

Figure 7. Temperature dependence of intrinsic triplet state lifetime for EGFP and rsEGFP2. Solid symbol data are mean ± SD from $n = 2$ datasets from fits to curves as in Figures 5 and 6; empty symbols are fits to phosphorescence decays as in Figure 1C. For $T > 220$ K, these curves are too noisy to extract meaningful lifetimes. (A) Linear presentation lifetime vs temperature. (B) Arrhenius presentation ln(1/lifetime) vs 1000/temperature of the same data (note that temperature increases from right to left in this presentation). The slope on the steep left half is four times smaller than at RT, on the flat right half 120 times, formally corresponding to activation barriers of 65 and 2.2 meV.

>50% and faster than 0.2 ms $^{-1}$ at power densities as moderate as 100 W cm^{-2}. Triplet state saturation thus leads to a considerable loss of detectable fluorescence intensity already at very moderate illumination levels. This loss, however, can be recovered within relatively short dark periods as also routinely applied in microscopy, e.g., for camera readout. The fact that both dark state formation and recovery happen on the same time scale as image acquisition by the camera provides an extraordinary sensitivity of observable photon count rates on camera and laser parameters as a consequence. Thus, in addition to standardized sample preparation and illumination schemes, a "standardized" acquisition timing is also important.

CONCLUSIONS

Combining fluorescence and phosphorescence kinetics, we have determined the spectrum and yields for light-induced formation and decay of the first excited triplet state of two GFPs upon continuous 488 nm laser excitation at CTs. Knowing these parameters, we can conclude on the importance of FISC and RISC between the singlet and triplet manifolds S ↔ T in photoswitchable (rsEGFP2) and non-photoswitchable (EGFP) GFPs for their population dependence on excitation energy flux, also at RT.

The concept of pulsed illumination to allow for T_1 relaxation (T-Rex), as proposed earlier for MHz excitation,[14] should be applicable in the millisecond illumination regime such as used in PALM-type super-resolution imaging as well.[27] By allowing for complete triplet state relaxation between subsequent excitation pulses (i.e., few ms at RT and few tens of ms at CT), the singlet-state population may be more than doubled, and this could provide hope for corresponding signal enhancement. This possibility is supported by the published reports of reduced bleaching at RT using pulsed illumination.[28] In the picture drawn here at CT, the triplet state T_1 acts, by analogy to what has been found at RT,[11] as the entrance gateway to further absorption and photochemistry. Then, the similarity of the parameters obtained for EGFP and rsEGFP2 suggests that a certain cryo switchability could also be expected for EGFP.[3,5,29] The similarity of the T_1 absorption spectrum at CT found here to that at RT introduced earlier[11] makes it a useful tool for performance optimization attempts such as tuning the excitation wavelength to maximize back-pumping from T_1 or additionally using specific infrared wavelengths. For GFP-type proteins at RT, the T_1 dark lifetime is shorter, but this is partly compensated for by the shift of the absorbance peak closer to the pump laser wavelength (488 nm), making light pumping non-negligible for even lower energy densities.

As the technique could also be applied to other FPs, knowledge of their T_1 spectrum would be very useful, e.g., primed photoconversion, RISC optimization, or the like.

https://doi.org/10.1021/acs.jpcb.3c02971
J. Phys. Chem. B XXXX, XXX, XXX−XXX

AUTHOR INFORMATION

Corresponding Author

Martin Byrdin − *Institut de Biologie Structurale, CNRS, Université Grenoble Alpes, CEA, IBS, 38044 Grenoble, France;* orcid.org/0000-0002-6389-8714; Email: martin.byrdin@ibs.fr

Authors

Lukas Rane − *Institut de Biologie Structurale, CNRS, Université Grenoble Alpes, CEA, IBS, 38044 Grenoble, France;* orcid.org/0000-0003-4609-2265

Jip Wulffele − *Institut de Biologie Structurale, CNRS, Université Grenoble Alpes, CEA, IBS, 38044 Grenoble, France*

Dominique Bourgeois − *Institut de Biologie Structurale, CNRS, Université Grenoble Alpes, CEA, IBS, 38044 Grenoble, France;* orcid.org/0000-0002-1862-7712

Oleksandr Glushonkov − *Institut de Biologie Structurale, CNRS, Université Grenoble Alpes, CEA, IBS, 38044 Grenoble, France*

Angela M. R. Mantovanelli − *Institut de Biologie Structurale, CNRS, Université Grenoble Alpes, CEA, IBS, 38044 Grenoble, France*

Ninon Zala − *Institut de Biologie Structurale, CNRS, Université Grenoble Alpes, CEA, IBS, 38044 Grenoble, France*

Complete contact information is available at: https://pubs.acs.org/10.1021/acs.jpcb.3c02971

Notes

The authors declare no competing financial interest.

ACKNOWLEDGMENTS

M.B. thanks Klaus Brettel, Saclay, for fruitful discussions. Virgile Adam and Arijit Maity (both Grenoble) are acknowledged for critical comments. This work was supported by ANR-17-CE11-0047-01 and an Impulsion grant by the French Commissariat for atomic and renewable energies. The IBS acknowledges integration into the Interdisciplinary Research Institute of Grenoble (IRIG, CEA).

REFERENCES

(1) Schwartz, C. L.; Sarbash, V. I.; Ataullakhanov, F. I.; McIntosh, J. R.; Nicastro, D. Cryo-Fluorescence Microscopy Facilitates Correlations between Light and Cryo-Electron Microscopy and Reduces the Rate of Photobleaching. *J. Microsc.* **2007**, *227*, 98−109.

(2) Hulleman, C. N.; Li, W.; Gregor, I.; Rieger, B.; Enderlein, J. Photon Yield Enhancement of Red Fluorophores at Cryogenic Temperatures. *ChemPhysChem* **2018**, *19*, 1774−1780.

(3) Tuijtel, M. W.; Koster, A. J.; Jakobs, S.; Faas, F. G. A.; Sharp, T. H. Correlative Cryo Super-Resolution Light and Electron Microscopy on Mammalian Cells Using Fluorescent Proteins. *Sci. Rep.* **2019**, *9*, 1369.

(4) Hoffman, D. P.; Shtengel, G.; Xu, C. S.; Campbell, K. R.; Freeman, M.; Wang, L.; Milkie, D. E.; Pasolli, H. A.; Iyer, N.; Bogovic, J. A.; Stabley, D. R.; Shirinifard, A.; Pang, S.; Peale, D.; Schaefer, K.; Pomp, W.; Chang, C.-L.; Lippincott-Schwartz, J.; Kirchhausen, T.; Solecki, D. J.; Betzig, E.; Hess, H. F. Correlative Three-Dimensional Super-Resolution and Block-Face Electron Microscopy of Whole Vitreously Frozen Cells. *Science* **2020**, *367*, No. eaaz5357.

(5) Mantovanelli, A. M. R.; Glushonkov, O.; Adam, V.; Wulffele, J.; Thédié, D.; Byrdin, M.; Gregor, I.; Nevskyi, O.; Enderlein, J.; Bourgeois, D. Photophysical Studies at Cryogenic Temperature Reveal a Novel Photoswitching Mechanism of RsEGFP2. *bioRxiv* **2022**, 504779 Posted August 22, 2022.

(6) Dahlberg, P. D.; Sartor, A. M.; Wang, J.; Saurabh, S.; Shapiro, L.; Moerner, W. E. Identification of PAmKate as a Red Photoactivatable Fluorescent Protein for Cryogenic Super-Resolution Imaging. *J. Am. Chem. Soc.* **2018**, *140*, 12310−12313.

(7) Regis Faro, A.; Carpentier, P.; Jonasson, G.; Pompidor, G.; Arcizet, D.; Demachy, I.; Bourgeois, D. Low-Temperature Chromophore Isomerization Reveals the Photoswitching Mechanism of the Fluorescent Protein Padron. *J. Am. Chem. Soc.* **2011**, *133*, 16362−16365.

(8) Dahlberg, P. D.; Moerner, W. E. Cryogenic Super-Resolution Fluorescence and Electron Microscopy Correlated at the Nanoscale. *Annu. Rev. Phys. Chem.* **2021**, *72*, 253−278.

(9) DeRosier, D. J. Where in the Cell Is My Protein? *Q. Rev. Biophys.* **2021**, *54*, No. e9.

(10) Orrit, M.; Bernard, J. Single Pentacene Molecules Detected by Fluorescence Excitation in a *p* -Terphenyl Crystal. *Phys. Rev. Lett.* **1990**, *65*, 2716−2719.

(11) Byrdin, M.; Duan, C.; Bourgeois, D.; Brettel, K. A Long-Lived Triplet State Is the Entrance Gateway to Oxidative Photochemistry in Green Fluorescent Proteins. *J. Am. Chem. Soc.* **2018**, *140*, 2897−2905.

(12) Widengren, J.; Mets, Ü.; Rigler, R. Photodynamic Properties of Green Fluorescent Proteins Investigated by Fluorescence Correlation Spectroscopy. *Chem. Phys.* **1999**, *250*, 171−186.

(13) Coquelle, N.; Sliwa, M.; Woodhouse, J.; Schirò, G.; Adam, V.; Aquila, A.; Barends, T. R. M.; Boutet, S.; Byrdin, M.; Carbajo, S.; et al. Chromophore Twisting in the Excited State of a Photoswitchable Fluorescent Protein Captured by Time-Resolved Serial Femtosecond Crystallography. *Nat. Chem.* **2018**, *10*, 31−37.

(14) Donnert, G.; Eggeling, C.; Hell, S. W. Major Signal Increase in Fluorescence Microscopy through Dark-State Relaxation. *Nat. Methods* **2007**, *4*, 81−86.

(15) Byrdin, M.; Bourgeois, D. The CAL(AI)2DOSCOPE: A Microspectrophotometer for Accurate Recording of Correlated Absorbance and Fluorescence Emission Spectra. *Spectrosc. Eur.* **2016**, *28*, 14−17.

(16) Patterson, G. H.; Knobel, S. M.; Sharif, W. D.; Kain, S. R.; Piston, D. W. Use of the Green Fluorescent Protein and Its Mutants in Quantitative Fluorescence Microscopy. *Biophys. J.* **1997**, *73*, 2782−2790.

(17) Grotjohann, T.; Testa, I.; Reuss, M.; Brakemann, T.; Eggeling, C.; Hell, S. W.; Jakobs, S. RsEGFP2 Enables Fast RESOLFT Nanoscopy of Living Cells. *eLife* **2012**, *1*, No. e00248.

(18) Keller, R. A. Excited Triplet — Singlet Intersystem Crossing. *Chem. Phys. Lett.* **1969**, *3*, 27−29.

(19) Ringemann, C.; Schonle, A.; Giske, A.; von Middendorff, C.; Hell, S. W.; Eggeling, C. Enhancing Fluorescence Brightness: Effect of Reverse Intersystem Crossing Studied by Fluorescence Fluctuation Spectroscopy. *Chemphyschem* **2008**, *9*, 612−624.

(20) Smit, R.; Ristanović, Z.; Kozankiewicz, B.; Orrit, M. Reverse Intersystem Crossing of Single Deuterated Perylene Molecules in a Dibenzothiophene Matrix. *ChemPhysChem* **2021**, *23*, No. e202100679.

(21) Mukherjee, S.; Jimenez, R. Photophysical Engineering of Fluorescent Proteins: Accomplishments and Challenges of Physical Chemistry Strategies. *J. Phys. Chem. B* **2022**, *126*, 735−750.

(22) Adam, V.; Hadjidemetriou, K.; Jensen, N.; Shoeman, R. L.; Woodhouse, J.; Aquila, A.; Banneville, A.; Barends, T. R. M.; Bezchastnov, V.; Boutet, S.; et al. Rational Control of Off-State Heterogeneity in a Photoswitchable Fluorescent Protein Provides Switching Contrast Enhancement. *ChemPhysChem* **2022**, *23*, No. e202200192.

(23) Lin, C.-Y.; Romei, M. G.; Oltrogge, L. M.; Mathews, I. I.; Boxer, S. G. Unified Model for Photophysical and Electro-Optical Properties of Green Fluorescent Proteins. *J. Am. Chem. Soc.* **2019**, *141*, 15250−15265.

(24) Weik, M.; Vernede, X.; Royant, A.; Bourgeois, D. Temperature Derivative Fluorescence Spectroscopy as a Tool to Study Dynamical Changes in Protein Crystals. *Biophys. J.* **2004**, *86*, 3176−3185.
(25) Duan, C.; Adam, V.; Byrdin, M.; Ridard, J.; Kieffer-Jaquinod, S.; Morlot, C.; Arcizet, D.; Demachy, I.; Bourgeois, D. Structural Evidence for a Two-Regime Photobleaching Mechanism in a Reversibly Switchable Fluorescent Protein. *J. Am. Chem. Soc.* **2013**, *135*, 15841−15850.
(26) Peng, B.; Dikdan, R.; Hill, S. E.; Patterson-Orazem, A. C.; Lieberman, R. L.; Fahrni, C. J.; Dickson, R. M. Optically Modulated and Optically Activated Delayed Fluorescent Proteins through Dark State Engineering. *J. Phys. Chem. B* **2021**, *125*, 5200−5209.
(27) Hess, S. T.; Girirajan, T. P. K.; Mason, M. D. Ultra-High Resolution Imaging by Fluorescence Photoactivation Localization Microscopy. *Biophys. J.* **2006**, *91*, 4258−4272.
(28) Shaner, N. C.; Lin, M. Z.; McKeown, M. R.; Steinbach, P. A.; Hazelwood, K. L.; Davidson, M. W.; Tsien, R. Y. Improving the Photostability of Bright Monomeric Orange and Red Fluorescent Proteins. *Nat. Methods* **2008**, *5*, 545−551.
(29) Kaufmann, R.; Schellenberger, P.; Seiradake, E.; Dobbie, I. M.; Jones, E. Y.; Davis, I.; Hagen, C.; Grünewald, K. Super-Resolution Microscopy Using Standard Fluorescent Proteins in Intact Cells under Cryo-Conditions. *Nano Lett.* **2014**, *14*, 4171−4175.

https://doi.org/10.1021/acs.jpcb.3c02971
J. Phys. Chem. B XXXX, XXX, XXX−XXX